J. Fluid Mech. (2008), *vol.* 605, *pp.* 401–428. © 2008 Cambridge University Press
doi:10.1017/S002211200800164X Printed in the United Kingdom

Acoustic resonances and trapped modes in pipes and tunnels

STEFAN HEIN AND WERNER KOCH
Institute of Aerodynamics and Flow Technology, DLR Göttingen, Germany

(Received 19 September 2007 and in revised form 12 March 2008)

Acoustic resonances of simple three-dimensional finite-length structures in an infinitely long cylindrical pipe are investigated numerically by solving an eigenvalue problem. To avoid unphysical reflections at the finite grid boundaries placed in the uniform cross-sections of the pipe, perfectly matched layer absorbing boundary conditions are applied in the form of the complex scaling method of atomic and molecular physics. Examples of the structures investigated are sound-hard spheres, cylinders, cavities and closed side branches. Several truly trapped modes with zero radiation loss are identified for frequencies below the first cutoff frequency of the pipe. Such trapped modes can be excited aerodynamically by coherent vortices if the frequency of the shed vortices is close to a resonant frequency. Furthermore, numerical evidence is presented for the existence of isolated embedded trapped modes for annular cavities above the first cutoff frequency and for closed side branches below the first cutoff frequency. As applications of engineering interest, the acoustic resonances are computed for a ball-type valve and around a simple model of a high-speed train in an infinitely long tunnel.

1. Introduction

In their survey paper Parker & Stoneman (1989) demonstrated that vortex shedding can be altered and enhanced dramatically by acoustic resonances in many engineering problems of practical importance. When the vortex shedding frequency is near an acoustic resonant frequency the former may lock on to the resonant frequency and the acoustic resonance may control the shedding process in a similar way to that observed with mechanical oscillations of bluff bodies in a flow, cf. Bearman (1984). In the locked-on state even fully turbulent flows show highly coherent vortices and the corresponding high-amplitude oscillations often cause damagingly high vibrations and/or unbearably loud noise. These high-amplitude oscillations can be controlled by either suppressing the vortex shedding or changing the geometry of the resonator. The former is more effective but not always possible. In this paper we are concerned with predicting dangerous resonances with low radiation damping, i.e. high quality factor Q, for a particular geometry of unbounded resonators. In the original experimental investigation of Parker (1966) the source exciting these acoustic resonances were von-Kármán-like coherent vortices generated in the self-excited wake behind a blunt-edged plate. However, similar lock-on effects were observed in finite-length side branches and pipes, see Dequand, Hulshoff & Hirschberg (2003) or Rockwell *et al.* (2003), where Rossiter-like feedback modes of impinging shear layers provide the source of excitation.

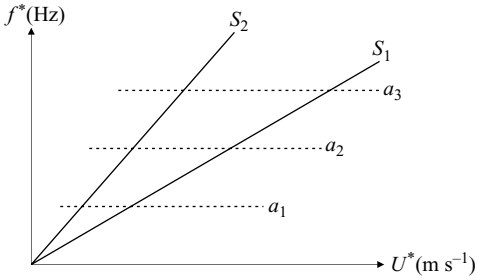

FIGURE 1. Frequency f^* versus flow velocity U^* for Strouhal sources S and acoustic resonances a (schematically).

Vortex shedding is a strictly hydrodynamical oscillation and usually follows a constant Strouhal number law, i.e. the shedding frequency f^* increases approximately linearly with flow velocity U^*. On the other hand the frequency of acoustic resonances for a given geometry is approximately constant, at least at low Mach numbers, as sketched in figure 1. Without acoustic resonance the frequency of the shed vortices follows the constant Strouhal lines for purely hydrodynamic oscillations denoted by S. For wakes only a single Strouhal line, for example S_1, is excited. For impinging shear layers, such as flows over cavities, several Strouhal lines are possible due to a feedback mechanism, see Rockwell & Naudascher (1979). As soon as the frequency of a Strouhal source line is close to an acoustic resonant frequency line, denoted by a, lock-on may occur with corresponding enhancement of the oscillation if the acoustic resonance has low damping. It is even possible that more than one resonance may be excited by a single Strouhal source, or that several Strouhal sources may lock on to a single resonance. Lock-on is a complicated nonlinear process which is not the subject of this investigation. But knowledge of the acoustic resonant frequencies gives us an idea of at which frequencies lock-on and possibly dangerously high oscillations might be expected.

Parker (1966) first observed acoustic resonances for a finite-length plate placed symmetrically between parallel duct walls and found that at the resonances the pressure decayed exponentially in the axial direction away from the plate. This enabled Parker (1967*b*) to compute the resonant frequencies by means of a numerical relaxation technique. The corresponding modes are often referred to as Parker's modes, see Nayfeh & Huddleston (1979). In the context of water waves Evans & Linton (1991) rediscovered Parker's modes and showed that they are truly trapped modes, i.e. with zero radiation loss and trapped near the structure in the laterally bounded duct. For the symmetrically placed plate Parker's trapped modes exist only below the cutoff frequency of the first antisymmetric duct mode. Therefore, excitation of these trapped modes by an incident wave of the same frequency is not possible according to linear theory (recently Li & Mei 2006 showed that these trapped modes could be excited subharmonically by an incident wave of twice the eigenfrequency). Resonances above the first duct cutoff frequency are damped due to radiation losses through the duct and a radiation condition has to be applied. However, Evans & Porter (1998) found theoretical evidence that isolated, so-called embedded trapped modes may also exist above the cutoff frequency under very special conditions. These modes are embedded in the continuous spectrum and therefore difficult to compute. Recently Duan *et al.* (2007) compared numerically obtained resonances with vanishingly small imaginary part with calculations based on semi-analytic methods

for simple structures in two-dimensional ducts and found excellent agreement between the two approaches. This demonstrates that a numerical search for resonances with vanishingly small radiation loss can aid in identifying trapped modes. Mathematically it is of importance to prove the existence of exactly trapped modes because it means the existence of an eigensolution to the homogeneous problem and therefore non-uniqueness of the inhomogeneous problem. However, for practical purposes it makes no difference whether the radiation loss is exactly zero or only very small because even nearly trapped modes with very low radiation loss can be excited by self-sustaining shear-layer oscillations.

The objective of the present paper is to extend the numerical method employed by Duan *et al.* (2007) to the computation of acoustic resonances in infinitely long pipes containing three-dimensional structures of finite length. Even though the sound sources are flow-excited, the resonances are computed for the no-flow situation assuming that the influence of flow on the resonances is negligible for low Mach number flows, see Koch (1983). Of special interest are resonances with vanishingly small damping which might correspond to trapped modes. We are aware of very few publications proving the existence of exactly trapped modes for three-dimensional structures in an infinitely long pipe with frequencies below the first pipe cutoff frequency. Examples are the classical paper by Ursell (1991) for a sufficiently small sphere in a pipe, and the extension to spheres of arbitrary size as well as to a cylindrical sleeve in a pipe by Linton & McIver (1998). Regarding embedded trapped modes with frequencies above the first pipe cutoff frequency, Linton & McIver (2007) state that they are not aware of any calculations for three-dimensional guides. In the present paper evidence is presented that embedded trapped modes may also exist for annular cavities or closed side branches in a pipe for special geometric parameters and frequencies. The existence of exactly trapped modes can only be proved for very special geometries. However, the numerical method of Hein, Hohage & Koch (2004) can be used to compute resonances in arbitrarily shaped domains as long as they end in infinitely long pipes of constant cross-section. In this way one can identify modes with vanishingly small damping as possible trapped modes if the damping approaches zero as the finite element grid is refined. Of course the solution of the discretized problem is limited by the relevant computational resources.

The paper is structured as follows: after a brief outline of the solution method in § 2 the acoustic resonances of several finite-length obstacles in an infinitely long circular cylindrical pipe are investigated in § 3. As engineering applications the acoustic resonances are computed for a ball-type valve and a high-speed train in an infinitely long tunnel. The acoustic resonances of cavities of finite axial extent as well as closed side branches in an infinite pipe are computed in § 4. The concluding section summarizes the various results.

2. Governing equation and solution procedure

The equation governing acoustic disturbances in a medium with zero mean flow is the wave equation. In the following all lengths will be non-dimensionalized with a characteristic reference length l^*_{ref}, velocities with the ambient speed of sound c^*_0, densities with the ambient density ρ^*_0, and pressures with $\rho^*_0 c^{*2}_0$. Here the asterisk superscript denotes a dimensional quantity. Assuming periodic time dependence $\exp(-\mathrm{i}\omega^* t^*)$, where ω^* is the circular frequency, the wave equation can be reduced to the Helmholtz equation

$$\Delta\phi(x, y, z) + K^2\phi(x, y, z) = 0 \tag{2.1}$$

for the (non-dimensional) velocity potential $\phi(x, y, z)$. $\Delta = \partial^2/\partial x^2 + \partial^2/\partial y^2 + \partial^2/\partial z^2$ is the three-dimensional Laplacian in (non-dimensional) Cartesian coordinates x, y, z and $K = \omega^* l^*_{ref}/c^*_0$ denotes the dimensionless frequency, with $K/2\pi$ being the Helmholtz number. The time-independent dimensionless disturbance velocity and pressure are then given by $\boldsymbol{v}(x, y, z) = \nabla\phi$ and $p(x, y, z) = \mathrm{i}K\phi$, respectively. On the solid pipe walls as well as on any obstacle we impose the Neumann boundary condition

$$\frac{\partial\phi}{\partial n} = 0 \tag{2.2}$$

for sound-hard walls.

A complex number K with $\mathrm{Im}(K) < 0$ is called a *resonance* if there exists a non-trivial solution ϕ to the eigenvalue equation (2.1) satisfying the Neumann boundary condition (2.2) and a radiation condition allowing only outgoing waves. Mathematically, resonances are equivalently defined as poles of the meromorphic extension of the resolvent of $-\Delta$ into the complex plane, see Hislop & Sigal (1996) or Taylor (1996). Numerical computations are necessarily conducted on truncated domains. At these finite grid boundaries unphysical reflections occur, often causing large errors in the solution, unless special boundary conditions are applied on the surface bounding the computational domain. Basically there are two methods to overcome this problem: the first uses so-called *non-reflecting boundary conditions* on the surface bounding the computational domain. Analysing the problem outside the truncated computational domain a relation can be established involving the unknown solution and its derivative. This so-called Dirichlet-to-Neumann (DtN) map is then used as boundary condition for the interior computational domain. Applications to wave guide problems can be found in Harari, Patlashenko & Givoli (1998) or Levitin & Marletta (2006).

The second method employs *absorbing boundary conditions* by adding a non-physical layer which absorbs outgoing waves without reflection. The so-called perfectly matched layer (PML) boundary conditions were introduced by Bérenger (1994) and became increasingly popular in electrodynamics and acoustics (for a recent review in acoustics see Hu 2004). In the complex coordinate stretching formulation of the PML, cf. Chew & Weedon (1994), the PML method is very similar to the much older *complex scaling method* of atomic and molecular physics. The complex scaling method was introduced by Aguilar & Combes (1971), Baslev & Combes (1971) and Simon (1973) and soon developed into an efficient computational tool, see Hislop & Sigal (1996) or the recent review by Moiseyev (1998). For wave guides with Dirichlet boundary conditions, so-called quantum wires, the method appears to have been proposed for the first time by Duclos, Exner & Šťovíček (1995). Duan *et al.* (2007) applied it to two-dimensional acoustic wave guide problems. Of particular importance are trapped modes which are defined as resonances with zero radiation loss. In a numerical method resonances with an imaginary part approaching zero can aid identification of trapped modes as demonstrated by Duan *et al.* (2007).

In the present paper we shall apply the complex scaling method to the computation of acoustic resonances in three-dimensional wave guides. The complex scaling method works as follows: in the PML domain $\phi(x, y, z)$ is continued analytically with respect to the axial variable x to the complex variable ξ, e.g.

$$\xi(x) = x + \mathrm{i}\sigma(x). \tag{2.3}$$

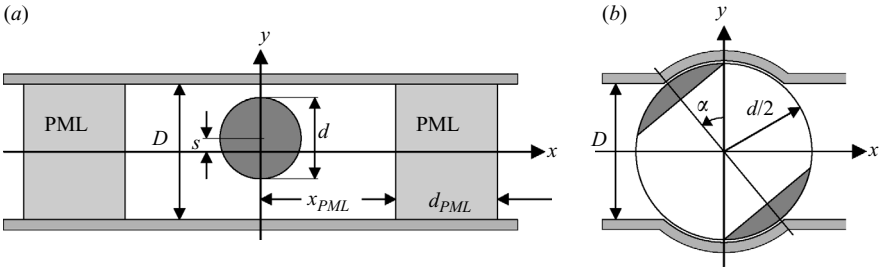

FIGURE 2. (*a*) Sphere in circular cylindrical pipe (with PMLs), (*b*) ball-type valve (without PMLs).

The spatial damping function $\sigma(x)$ is usually chosen in power form, smoothly starting at the PML interface at $x = \pm x_{PML}$:

$$\sigma(x) = \begin{cases} \sigma_0 (x - x_{PML})^\beta, & x > x_{PML}, \\ 0, & |x| \leqslant x_{PML}, \\ -\sigma_0 (-x - x_{PML})^\beta, & x < -x_{PML}. \end{cases} \tag{2.4}$$

For a positive damping coefficient σ_0 and a constant shape parameter $\beta \geqslant 1$ (we chose $\beta = 1$ for all our computations, cf. Hein *et al.* 2004) outgoing waves will decay exponentially in the PML. One can therefore truncate the PML at $\pm(x_{PML} + d_{PML})$, where d_{PML} denotes the width of the PML, see figure 2(*a*). The error due to artificial reflections at this truncated outer edge of the PML is small if σ_0 and d_{PML} are chosen properly (in general we chose $\sigma_0 = 1$ and $d_{PML} \geqslant 4$). Therefore, a Dirichlet boundary condition can be imposed at the outer edge of the PML instead of enforcing the radiation condition, cf. Collino & Monk (1998). A finite-domain eigenvalue problem results which can be solved numerically by standard codes. In this paper we apply the high-order finite-element code NGSolve of Joachim Schöberl together with his grid generation code NETGEN (Schöberl 1997), and solve the ensuing large eigenvalue problem with a shifted Arnoldi algorithm. The accuracy of the finite-element solution is controlled by the maximal mesh size Δ of the grid and the order p of the finite-element polynomial on an individual triangle. For three-dimensional objects the number of degrees of freedom N_{dof} in the finite-element formulation, and correspondingly the storage requirements, are quite large such that we use $p = 2$ in almost all our calculations. For occasional accuracy checks we increase p to $p = 3$ or $p = 4$. In NGSolve the mesh size Δ can be varied locally. For example we chose a much coarser mesh in the PML.

3. Obstacles in a cylindrical pipe

Trapped modes are to be expected around localized features in a wave guide, which we take to be a circular cylindrical pipe of constant diameter D^*. Then D^* is the natural reference length l^*_{ref} and $K = \omega^* D^*/c_0^*$. The first feature we investigate is a finite-length three-dimensional obstacle in a circular cylindrical pipe. Usually these objects are convex, but they need not be as demonstrated by the model of a ball-type valve, see figure 2(*b*), also treated in this section.

3.1. *Sphere in a circular cylindrical pipe*

For the two-dimensional problem of a hard-walled cylinder placed midway between two parallel plates Callan, Linton & Evans (1991) proved the existence of trapped

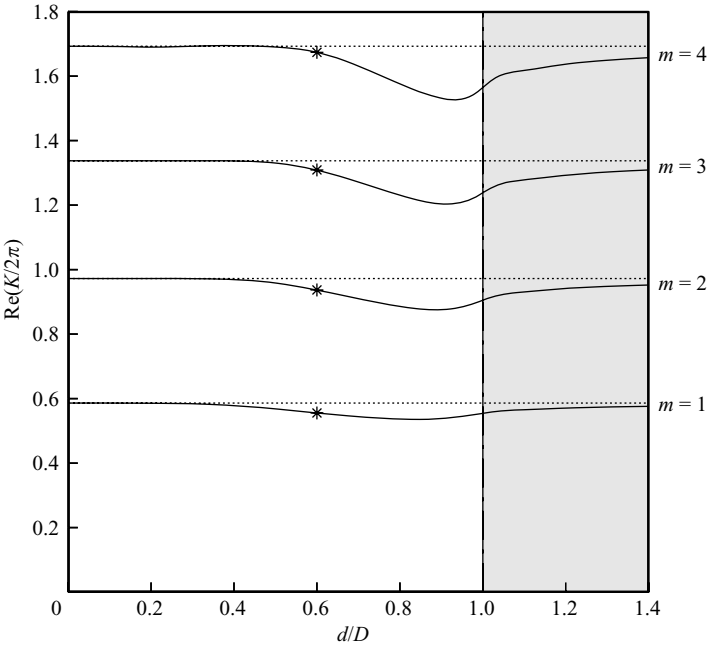

FIGURE 3. Centred sphere in pipe: frequencies of first four x-symmetric trapped modes $m = 1, \ldots, 4$ as a function of d/D computed with $p = 2$, $d_{PML} = 6$, $\sigma_0 = 1$, $\Delta = 0.04/0.12$ (the second number always indicates the Δ used in the PML).

modes. Ursell (1991) extended this proof to three dimensions, i.e. a hard-walled sphere of diameter d located on the axis ($s = 0$) of a hard-walled, circular cylindrical pipe of diameter D, figure 2(a). Using multipole expansions Ursell (1991) proved that a trapped mode exists with no radiation to infinity provided the sphere is sufficiently small and the wavenumber is near to (and below) the cutoff wavenumber of the pipe. Linton & McIver (1998) extended Ursell's proof to spheres of arbitrary size and showed that an infinite sequence of trapped circumferential modes exists whose wavenumbers tend to infinity. However, as far as we know, no computation of the trapped mode frequencies has been published up to now. In the following we shall compute the acoustic resonances for this problem numerically and, with the existence of trapped modes established theoretically, we identify the numerically obtained complex resonances with vanishingly small damping as Ursell's trapped modes.

Taking advantage of symmetries about $x = 0$ and $z = 0$ we limit the computational domain to the quarter-problem $x \geqslant 0$, $z \geqslant 0$. Figure 3 shows the frequencies of the first four circumferential trapped modes, marked $m = 1, \ldots, 4$. Here m denotes the circumferential mode number and the dotted lines mark the respective cutoff frequencies. Samples of the eigenfunctions $\mathrm{Re}(\phi)$ on the surface of the quarter-problem for $d/D = 0.6$, corresponding to the conditions marked by asterisks in figure 3, are depicted in figure 4. The line at $d/D = 1$ in figure 3 marks the limiting case when the sphere touches the pipe wall. For $d/D > 1$, marked by the shaded area, the sphere separates the pipe into two disconnected semi-infinite pipes with a spherical bottom. For the sphere all trapped modes appear to be symmetric in x. For longer structures antisymmetric trapped modes are also possible as demonstrated in § 3.3 for a finite-length cylinder. For a centred sphere the resonances which are symmetric and antisymmetric in z have the same trapped mode frequency; only the

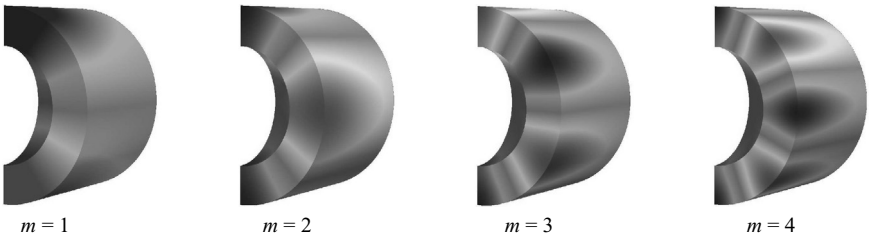

FIGURE 4. Centred sphere in pipe with $d/D = 0.6$: eigenfunctions of first four x-symmetric trapped modes $m = 1, \ldots, 4$ marked by asterisks in figure 3. Depicted are the eigenfunctions $\mathrm{Re}(\phi)$ on the surface of the quarter-problem $x \geqslant 0$, $z \geqslant 0$ up to $x_{PML} = 1$.

corresponding eigenfunctions are phase shifted by 90°. All computations in figure 3 were performed with $p = 2$. Increasing the polynomial order to $p = 3$ for several selected points reduced the imaginary part $\mathrm{Im}(K/2\pi)$ of the resonant frequencies to 10^{-7}, strongly indicating that these are indeed truly trapped modes.

Next we allow the centre of the sphere to move a distance s away from the centreline of the pipe. But, before investigating the three-dimensional case of the sphere we follow the suggestion of a referee and compute for comparison the two-dimensional case of a cylinder of diameter d in a two-dimensional waveguide formed by two parallel plates a distance h apart (in the two-dimensional case K is defined as $K = \omega^* h^*/c_0^*$). For this case Aslanyan, Parnovski & Vassiliev (2000) proved that the real trapped mode eigenvalue transforms into a complex resonance as the cylinder moves off-centre. Figure 5 shows our corresponding numerical results for $d/h = 0.6$, clearly demonstrating the transformation of the trapped mode into a resonance with radiation loss. At $s/h = 0.2$ the cylinder touches the waveguide wall and for $s/h > 0.2$ (marked by the shaded area in figure 5) the cylinder penetrates the wall resulting in a circular protrusion on one waveguide wall. Near $s/h = 0.2$ the resonance frequency approaches the first cutoff frequency depicted by the dotted line in figure 5(a). Unfortunately, near a cutoff frequency our numerical method encounters a basic difficulty because the wave propagates almost parallel to the edge of the perfectly matched layer (shown as PML for example in figure 2(a)) which makes the PML ineffective. Increasing the length d_{PML} of the PML helps, as can be seen in figure 5(b), but another problem is encountered which has been discussed in Duan *et al.* (2007): resonances are members of the discrete spectrum. At the cutoff frequencies continuous spectra start, which are approximated by discrete eigenvalues in our numerical approach. These discrete numerical eigenvalues, which are strongly dependent on the PML parameters, can be mistaken as resonant eigenvalues near a cutoff frequency and it becomes practically impossible to distinguish the two. Therefore, for $s/h > 0.2$ we do not consider the damping values in figure 5(b) to be accurate. However, the resonant frequency in figure 5(a) changes very little.

Now we return to the three-dimensional case and displace the centre of the sphere by a distance s from the axis of the pipe, say along the y-direction normal to the axis of the pipe, which is taken to be the x-coordinate. For the centred sphere the trapped modes are double eigenvalues (see also Linton & McIver 1998, p. 403), and by moving the centre of the sphere away from the axis of the pipe the trapped mode frequencies split into two eigenfrequencies as shown in figure 6(a) for $m = 1$. The resonance belonging to the mode symmetric in z (depicted by the solid and dash-dotted curves) shows a behaviour similar to that of the damped resonance in the above two-dimensional case. However, the radiation damping of the z-antisymmetric

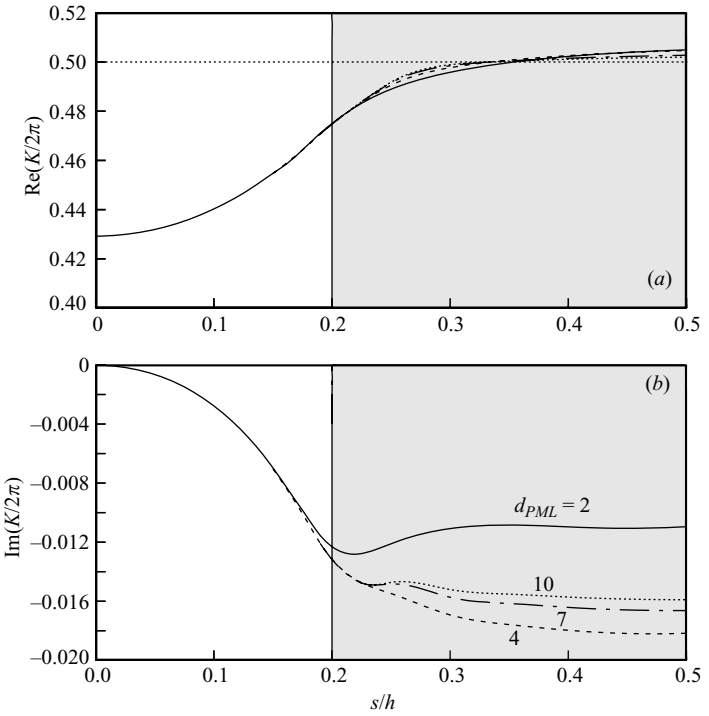

FIGURE 5. Cylinder in two-dimensional waveguide with $d/h = 0.6$: (a) variation of resonant frequency $\mathrm{Re}(K/2\pi)$ and (b) damping $\mathrm{Im}(K/2\pi)$ with off-centre distance s/h computed with $p = 6$, $\sigma_0 = 1$, $\Delta = 0.08$ and various d_{PML}.

mode (depicted by the dashed curve) is much lower than that of the z-symmetric mode, to the extent that the z-antisymmetric modes might even be truly trapped modes (with our numerical method we cannot prove this, but the imaginary part $\mathrm{Im}(K/2\pi)$ was found to be 10^{-10} for some s/D). This is strikingly different from the two-dimensional case and apparently due to the symmetry property about $z = 0$. At $s/D = 0.2$ the sphere with $d/D = 0.6$ touches the wall and the z-symmetric $m = 1$ mode frequency approaches the $m = 1$ cutoff frequency depicted by the dotted line in figure 6(a). For $s/D > 0.2$ (marked by the shaded area in figure 6) the sphere penetrates the wall of the pipe, constituting a hump-like obstacle on the pipe wall. As for the two-dimensional case the PML computation fails near $s/D = 0.2$ for the z-symmetric mode as demonstrated by the large difference between the two curves for the PML parameters $\sigma_0 = 1$ and 0.5 in figure 6(b).

3.2. *Ball-type valve in a circular cylindrical pipe*

If we consider a sphere in the pipe with a diameter $d/D = \sqrt{2}$ and drill a hole of diameter D through the sphere we obtain a simple model of a ball-type valve as depicted in figure 2(b). The valve angle $\alpha = 0^\circ$ denotes the completely open valve position and at $\alpha = 90^\circ$ the valve is completely closed. The real and imaginary parts of the resonant frequencies computed with $p = 2$ are shown in figure 7. The results are qualitatively similar to the results for the two-dimensional model presented in Duan *et al.* (2007) with the exception that additional circumferential modes appear. For the completely closed position $\alpha = 90^\circ$ the resonances converge to the real resonances of a circular cylindrical cavity with a spherical cap at both ends. For the computation

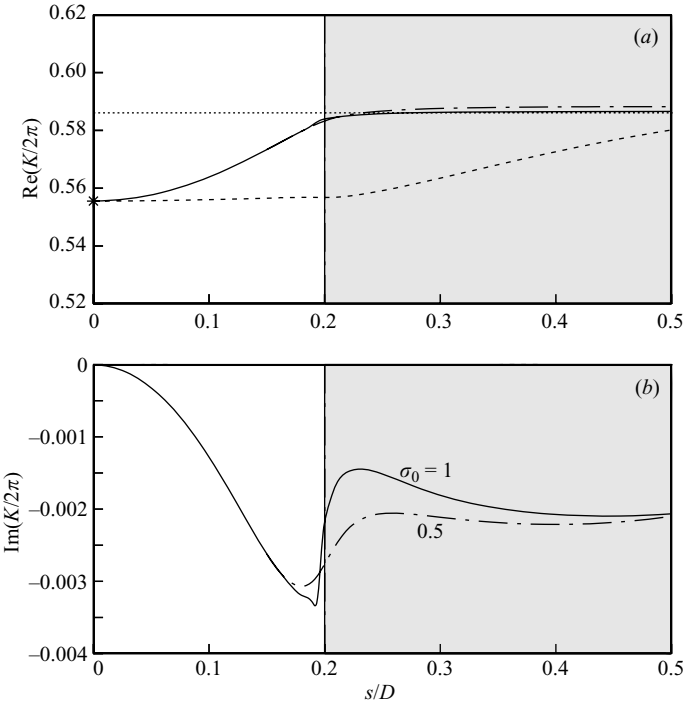

FIGURE 6. Sphere in pipe with $d/D = 0.6$: (a) variation of resonant frequency $\mathrm{Re}(K/2\pi)$ and (b) damping $\mathrm{Im}(K/2\pi)$ of the $m = 1$ modes with off-centre distance s/D. The solid curve depicts the z-symmetric $m = 1$ mode and the dashed curve the z-antisymmetric $m = 1$ mode computed with $p = 2$, $d_{PML} = 6$, $\sigma_0 = 1$, $\Delta = 0.04/0.12$. The dash-dotted curve shows the z-antisymmetric $m = 1$ mode computed with $\sigma_0 = 0.5$. The dashed curve in (b) coincides with the abscissa within drawing accuracy.

of the resonances in this closed cavity we can take advantage of symmetries in the three coordinates. The corresponding cavity resonance frequencies are marked by the arrows on the right-hand side of figure 7(a) and are labelled according to the symmetry (S) or antisymmetry (A) of the eigenfunction ϕ in x, y, z respectively. Most of the resonances quickly reach high damping as the valve is opened. Only the mode depicted by the solid curve seems to become a nearly trapped mode with very low damping in the vicinity of $\alpha = 45^\circ$ and therefore might be expected to cause the largest noise when excited by shear layers. Increasing p to $p = 4$ did not reduce the imaginary part of this mode noticeably, indicating that it is not a truly trapped mode. The resonant mode starting as SAS, depicted by the dash-dotted curve, reaches maximal damping near $\alpha = 30^\circ$ and then approaches the first cutoff frequency of the pipe depicted by the horizontal line in figure 7(a).

3.3. *Finite-length cylinder in a circular cylindrical pipe*

As a third example we consider a hard-walled circular cylinder of length l and diameter d placed in a hard-walled circular cylindrical pipe of diameter D. The axis of the cylinder is aligned with the pipe axis but shifted by an amount s in the y-direction, see figure 8. First we investigate the case with $s = 0$, i.e. a concentric cylinder. For the case of axisymmetric hard-walled obstacles on the axis of a circular cylindrical pipe of constant cross-section Linton & McIver (1998) proved the existence of an infinite sequence of trapped circumferential modes. Similar to the existence proof

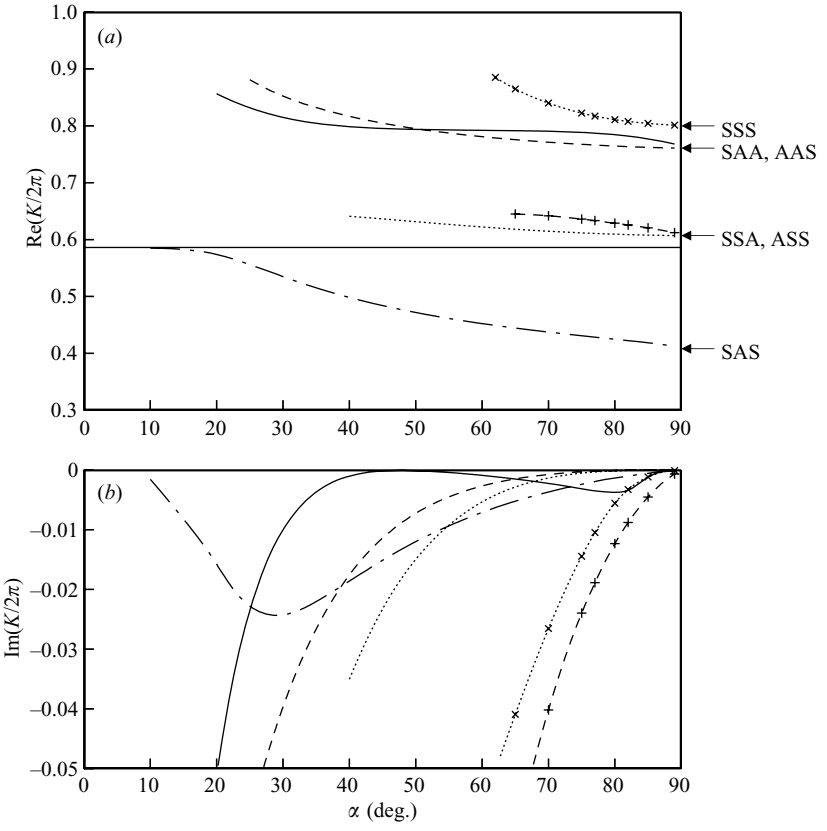

FIGURE 7. Resonances of ball-type valve as a function of valve angle α: (*a*) resonant frequency $\mathrm{Re}(K/2\pi)$ and (*b*) damping $\mathrm{Im}(K/2\pi)$ of first few resonances computed with $p = 2$, $d_{PML} = 5$, $\sigma = 1$, $\Delta = 0.08/0.2$.

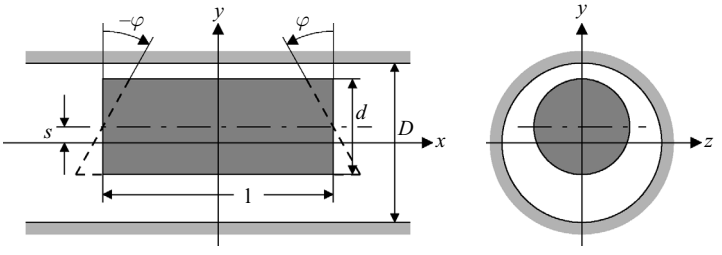

FIGURE 8. Circular (chamfered) cylinder of finite length placed eccentrically in a circular pipe.

of Ursell (1991), Linton & McIver (1998) introduced a cutoff by considering modes of a particular angular variation

$$\phi(x, r, \theta) = \hat{\phi}(x, r)\cos(m\theta). \tag{3.1}$$

As an example Linton & McIver (1998) computed the trapped mode frequencies for an infinitely thin circular sleeve placed concentrically in a circular pipe by means of the mode matching technique of Mittra & Lee (1971). In this section, instead of the circular sleeve we consider a hard-walled circular cylinder and compute the complex resonances numerically using PMLs. The common axis of the pipe and the cylinder

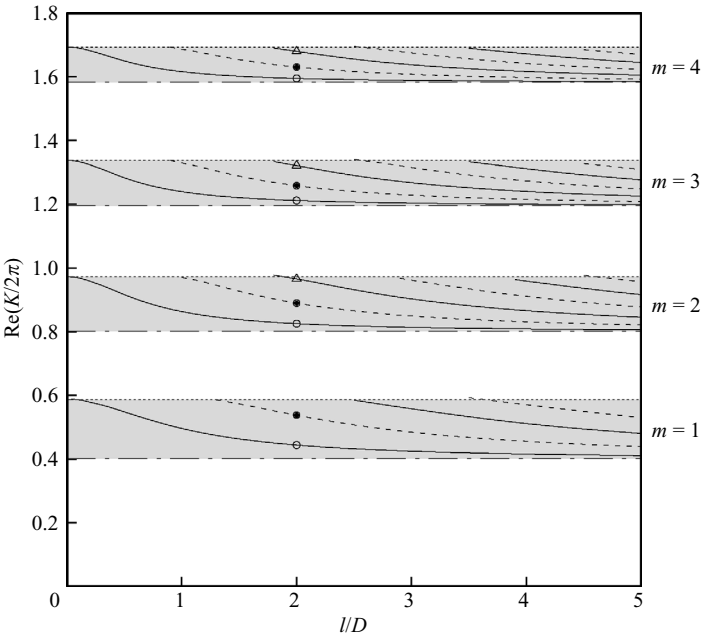

FIGURE 9. Axisymmetric solid cylinder with $d/D = 0.6$ in pipe: variation of x-symmetric (even n, solid curves) and x-antisymmetric (odd n, dashed curves) trapped mode frequencies as a function of cylinder length l/D computed with $p = 2$, $d_{PML} = 4$, $\sigma_0 = 1$, $\Delta = 0.04/0.16$.

FIGURE 10. Finite-length cylinder centred in pipe with $d/D = 0.6$ and $l/D = 2$: sample eigenfunctions (m, n, ρ) of x-symmetric and x-antisymmetric trapped modes. Depicted are the eigenfunctions $\mathrm{Re}(\phi)$ on the surface of the quarter-problem $x \geqslant 0$, $z \geqslant 0$ up to $x_{PML} = 1.5$.

is taken to be the x-coordinate. For the actual computation we take advantage of symmetries about $x = 0$ and $z = 0$ and limit our domain again to the quarter-problem $x \geqslant 0$, $z \geqslant 0$. Identifying complex resonances with vanishingly small imaginary part as trapped modes the trapped mode frequencies of the first four circumferential trapped modes $m = 1, \ldots, 4$ are depicted in figure 9 as a function of cylinder length l/D for the particular value $d/D = 0.6$. The results are very similar to the results for the sleeve presented in figure 1 of Linton & McIver (1998).

For axisymmetric obstacles on the centreline it is advantageous to distinguish resonant modes by three numbers (m, n, ρ). Here m is the circumferential mode number, and n and ρ denote the number of nodal lines in the axial and radial direction respectively. The solid curves in figure 9 depict the trapped mode frequencies of the modes symmetric about $x = 0$, i.e. $n = 0, 2, \ldots$; the dashed curves show the antisymmetric mode frequencies, i.e. $n = 1, 3, \ldots$. Sample eigenfunctions on the surface of the quarter-problem $x \geqslant 0$, $z \geqslant 0$ are shown in figure 10 for $l/D = 2$, marked by the various symbols in figure 9. Clearly, the trapped modes exist only in

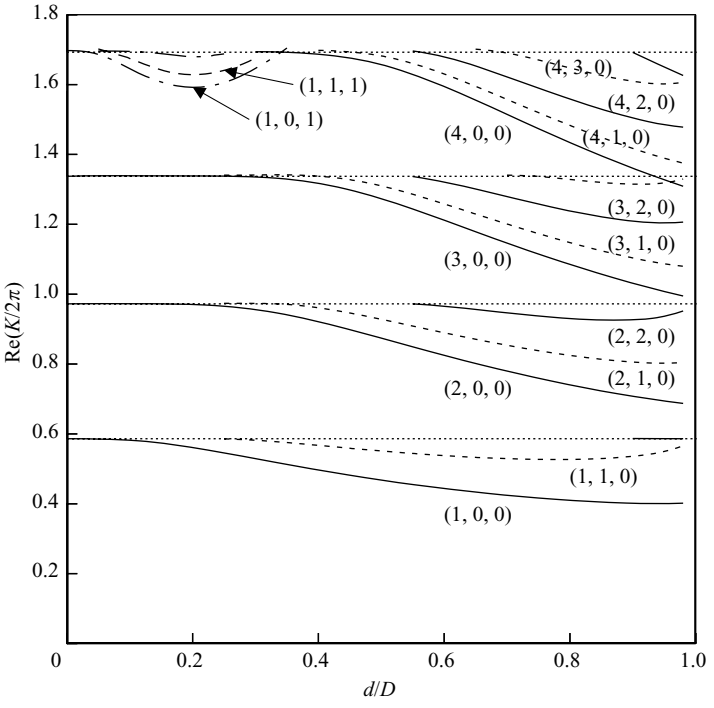

FIGURE 11. Finite-length cylinder with $l/D = 2$ centred in pipe: variation of (m, n, ρ) trapped mode frequencies as a function of d/D computed with $p = 2$, $d_{PML} = 4$, $\sigma_0 = 1$, $\Delta = 0.04/0.16$.

the shaded domains between the cutoff frequencies of the empty pipe (dotted lines) and the cutoff frequencies of the annular pipe with $d/D = 0.6$ (dash-dotted lines), similar to the circular sleeve results of Linton & McIver (1998).

Keeping $l/D = 2$ fixed we now vary d/D as in figure 2 of Linton & McIver (1998) for the cylindrical sleeve problem. The trapped mode frequencies are shown in figure 11 with the modal numbers (m, n, ρ) appended. The frequency curves are very similar to those for the cylindrical sleeve of Linton & McIver (1998). However, we have included the $m = 4$ modes and notice the appearance of the first radial trapped modes $\rho = 1$. For the empty pipe the cutoff frequency of the first radial mode, namely $\mathrm{Re}(K/2\pi) = 1.69705$, is very close to the cutoff frequency of the fourth circumferential mode, namely $\mathrm{Re}(K/2\pi) = 1.69263$.

Linton & McIver's (1998) existence proof of trapped modes applies only to centred axisymmetric objects. If the cylinder is no longer axisymmetric, for example by chamfering as indicated by the dashed lines in figure 8, or displacing the axis of the cylinder, i.e. $s \neq 0$, one expects the trapped modes to become damped resonances. To investigate this we look first at a cylinder with $s = 0$ but chamfered symmetrically on both ends (as indicated by the dashed lines in figure 8) such that we still may apply symmetry arguments with respect to $x = 0$ and $z = 0$. The results for $d/D = 0.6$ and $l/D = 2$ are depicted in figure 12 for the first x-symmetric ($n = 0$) and first x-antisymmetric ($n = 1$) mode starting with the $m = 1$ modes marked by the same symbols as in figure 9. The trapped modes of figure 9 are double resonances and split into z-symmetric and z-antisymmetric modes for $\varphi \neq 0$. Whereas the z-antisymmetric modes remain practically undamped, the z-symmetric modes become quickly damped

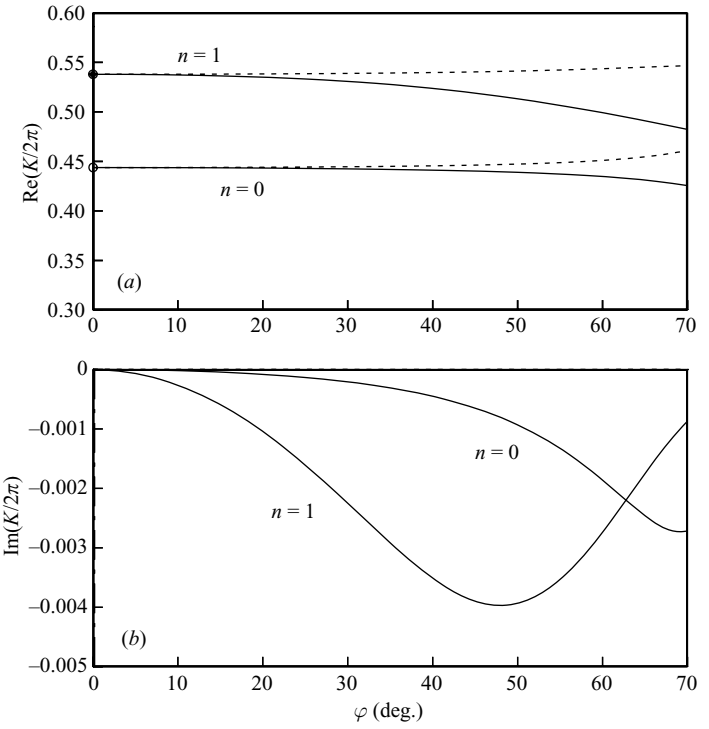

FIGURE 12. Chamfered finite-length cylinder with $d/D = 0.6$ and $l/D = 2$ centred in pipe: variation of (*a*) resonant frequency $\mathrm{Re}(K/2\pi)$ and (*b*) damping $\mathrm{Im}(K/2\pi)$ of the $m = 1$ modes with the angle φ of the chamfering plane. The solid curves depict the z-symmetric modes and the dashed curves the z-antisymmetric modes computed with $p = 2$, $d_{PML} = 4$, $\sigma_0 = 2$, $\Delta = 0.08/0.16$. The dashed curves in (*b*) coincide with the abscissa within drawing accuracy.

as φ increases. Near $\varphi = 70^\circ$ the chamfering plane cuts the cylinder close to the symmetry plane $x = 0$.

Next we displace the axis of the axisymmetric inner cylinder in the y-direction by a distance s as sketched in figure 8. Again, the marked trapped mode eigenvalues of figure 9 split into z-symmetric and z-antisymmetric resonances for $s > 0$. The corresponding results for the $m = 1$ modes with $d/D = 0.6$ and $l/D = 2$ are shown in figure 13. At $s/D = 0.2$ the inner cylinder touches the pipe wall and for $s/D > 0.2$ (marked by the shaded domain in figure 13) penetrates the pipe wall and acts like a cylindrical hump on the wall. Again one would expect that with increasing s all trapped modes become damped resonances. Whereas this seems to be the case for the z-symmetric modes (solid curves in figure 13), the z-antisymmetric modes (dashed curves in figure 13) are almost undamped. The z-symmetric $n = 0$ and $n = 1$ modes approach the first cutoff frequency (shown in figure 13(*a*) by the dotted line) from below for $s/D < 0.2$. For $s/D > 0.2$ higher z-symmetric n modes exist above the first cutoff frequency but they are highly damped as can be seen in figure 13(*b*) for the least damped $n = 2$ mode. Near the cutoff frequency the PML computation becomes inaccurate. The dotted curves in figure 13(*b*) are computed by doubling the thickness of the PML, i.e. $d_{PML} = 8$, and the slight deviations near the cutoff frequency indicate that the solution has not converged there.

As mentioned before, all trapped mode eigenvalues of figure 9 are double eigenvalues and the corresponding eigenfunctions are identical but phase-shifted by

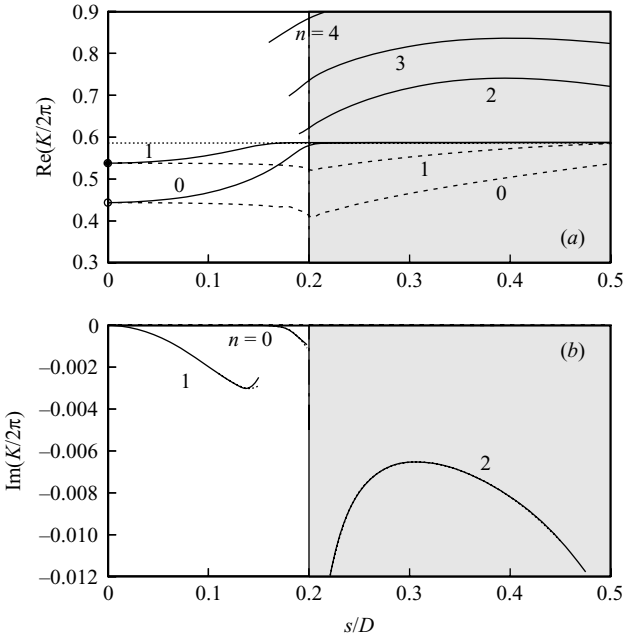

FIGURE 13. Finite-length cylinder with $d/D = 0.6$ and $l/D = 2$ in pipe: variation of (a) resonant frequency $\mathrm{Re}(K/2\pi)$ and (b) damping $\mathrm{Im}(K/2\pi)$ of the $m = 1$ modes with the off-centre distance s/D. The solid curves depict the z-symmetric modes and the dashed curves the z-antisymmetric modes computed with $p = 2$, $d_{PML} = 4$, $\sigma_0 = 1$, $\Delta = 0.08/0.16$. The dashed curves in (b) coincide with the abscissa within drawing accuracy.

90°, i.e. the eigenvalues have algebraic and geometric multiplicity 2. Superimposing two such eigenfunctions one obtains trapped acoustic spinning modes, cf. Parker (1984) or Duan & McIver (2004). If the effect of compressor blades is included, as in Duan & McIver (2004), these acoustic spinning mode resonances can enhance rotating sources caused by vortex shedding from blade rows. Experimentally such acoustic resonances were observed by Parker (1967*a*) for a single-stage compressor and Camp (1999) for a multi-stage compressor. Distinctive characteristics of these acoustic resonances in compressors are step changes with approximately constant frequency as the shaft speed changes, and large-amplitude pressure fluctuations accompanied by loud tones at lock-on.

3.4. *High-speed train in an infinitely long tunnel*

The existence of nearly trapped modes for non-axisymmetric obstacles in a pipe, discussed in the previous section, suggest investigating acoustic resonances of a finite-length high-speed train in an infinitely long tunnel. It is well known (see Diedrichs, Krajnović & Berg 2008 or Suzuki 2004 and literature cited therein) that the Japanese Series 300 Shinkansen showed large aerodynamically induced lateral vibrations of the tail vehicle in double-track tunnels. These lateral vibrations of about 2 Hz occurred at a speed of 300 km h^{-1} causing poor ride comfort. On the other hand, European high-speed trains such as the German Inter-City Express 2 (ICE 2) did not show these tail vehicle oscillations. Using large-eddy simulations (LES) of the flow about two simplified models of these high-speed trains in double-track tunnels Diedrichs *et al.* (2008) traced this difference in behaviour to the much stronger coherent wake-flow

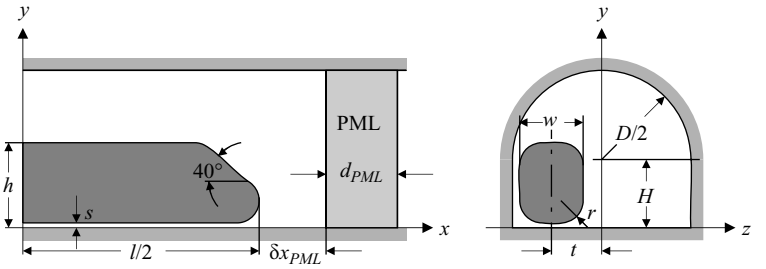

FIGURE 14. High-speed train model in an infinitely long double-track tunnel.

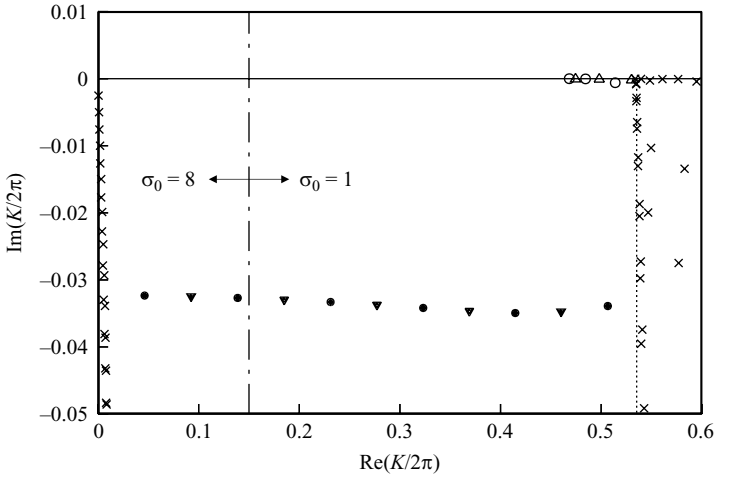

FIGURE 15. Sample resonance spectrum of our high-speed train model with two traction units and two middle wagons in a double-track tunnel computed with $p = 2$, $\sigma_0 = 8$ or 1, $d_{PML} = 12$, $\delta x_{PML} = 0.5$. The open symbols mark the nearly trapped resonances and the filled symbols mark the highly damped surface-wave resonances. Circles denote x-symmetric modes and triangles denote x-antisymmetric modes.

structures generated by the more rounded tail sides of the Shinkansen 300. If the acoustic resonances of the high-speed train in a tunnel are weakly damped and close to the frequency of excitation they could enhance these oscillations. Therefore, we compute in the following the acoustic resonances of a simplified high-speed train model in an infinitely long tunnel assuming that details such as running gears, underbelly equipment or inter-vehicle gaps are negligible.

Figure 14 shows a sketch of the simplified high-speed train model in an infinitely long tunnel. The main dimensions are chosen as follows: $D^* = 8.5\,\mathrm{m}$, $H^* = 3.25\,\mathrm{m}$, $t^* = 2.39\,\mathrm{m}$, $s^* = 0.232\,\mathrm{m}$, $h^* = 4.05\,\mathrm{m}$ and $w^* = 3.02\,\mathrm{m}$. The radius r^* is assumed to be $r^* = 0.58\,\mathrm{m}$ and the reference length l^*_{ref} is chosen to be the tunnel diameter D^*. The total length of the train is l^* and we assume symmetry or antisymmetry about $x = 0$ such that we may limit our computation to the half-problem $x \geqslant 0$. The train consists of a traction unit 20.56 m long at both ends of the train and N middle wagons, each of which is 26.4 m long.

A typical spectrum for two traction units with two middle wagons is depicted in figure 15. We note that between the continuous spectra of the fundamental mode frequency near $\mathrm{Re}(K/2\pi) = 0$ and the first tunnel cutoff frequency, marked by the dotted line, there exist two families of resonances: the open circular and triangular

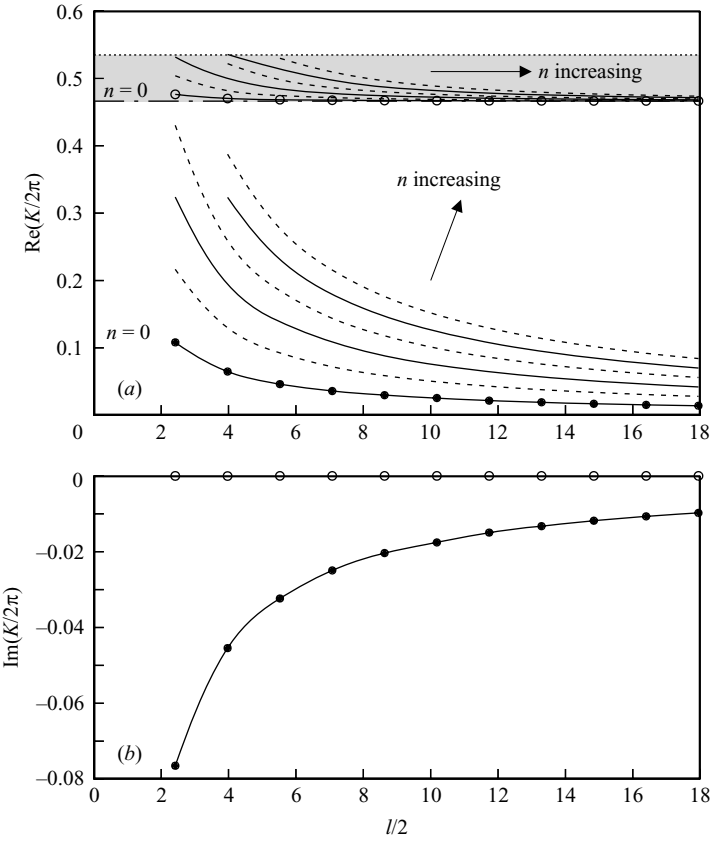

FIGURE 16. High-speed train model in a double-track tunnel as a function of half-train length $l/2$ computed with $p = 2$, $\sigma_0 = 2$, $d_{PML} = 2$, $\delta x_{PML} = 0.5$. (*a*) Resonant frequencies $\mathrm{Re}(K/2\pi)$, (*b*) damping $\mathrm{Im}(K/2\pi)$. The open symbols mark the nearly trapped resonant modes for $n = 0$ and the filled symbols mark the highly damped surface-wave resonances for $n = 0$, starting with $N = 0$ middle wagons up to $N = 10$ middle wagons.

symbols depict nearly trapped resonances below the first tunnel cutoff frequency, whereas the filled symbols mark highly damped surface-wave resonances similar to the two-dimensional surface-wave resonances described by Hein *et al.* (2007). The eigenfunctions of the present three-dimensional surface-wave resonances are almost uniform around the cross-section of the train but have n nodal lines in the axial direction starting with $n = 0$ at $\mathrm{Re}(K/2\pi) = 0.0463$. The surface-wave resonances radiate via the fundamental tunnel mode and are highly damped, all having approximately the same damping. The nearly trapped resonances resemble the truly trapped modes of the axisymmetric cylinder depicted in figure 9. They exist only below the first cutoff frequency of the empty tunnel and above the cutoff frequency of the tunnel containing an infinitely long train. The spectrum in figure 15 is patched together from two overlapping spectra with $\sigma_0 = 8$ and $\sigma_0 = 1$ at $\mathrm{Re}(K/2\pi) = 0.15$, marked by the dash-dotted vertical line. In this way the discrete members of the continuous spectra (due to our numerical discretization) cannot be confused with the true resonances marked by the circular and triangular symbols.

Figure 16 depicts the resonant frequency and damping of the two families of resonances as a function of the train half-length $l/2$. The x-symmetric $n = 0$

resonances are marked by symbols (open circles for the first nearly trapped resonance and filled circles for the first surface-wave resonance). Here the first symbol at $l/2 = 2.4188$ marks the length of the traction unit, i.e. $N = 0$. Each additional middle wagon up to $N = 10$ is depicted by a further symbol with increasing $l/2$. The resonances of the nearly trapped modes are in the shaded area of figure 16(*a*) below the first tunnel cutoff frequency (marked by the dotted line) and above the first cutoff frequency of the tunnel containing an infinitely long train (marked by the dash-dotted line). For long trains the latter cutoff frequency $\mathrm{Re}(K/2\pi) = 0.4662$ is approached by all nearly trapped modes. The corresponding eigenfunctions have n nodal lines in the axial direction but have different signs on the tunnel wall side and the tunnel centre side of the train. Therefore, they could enhance lateral vibrations. However, with $K/2\pi = 0.4662$, $D^* = 8.5\,\mathrm{m}$ and $c_0^* = 340\,\mathrm{m\,s^{-1}}$ the corresponding frequency is $f^* \approx 18\,\mathrm{Hz}$, which is an order of magnitude higher than the frequency of the observed lateral vibrations of the Shinkansen 300. The frequencies of the surface-wave resonances have the correct order of magnitude but could only enhance almost axisymmetric wake fluctuations. Furthermore, even though the damping of the surface-wave resonances decreases with increasing train length, the quality factor $Q = |\mathrm{Re}(K)/2\,\mathrm{Im}(K)|$ seems too low for strong enhancement. Exploratory computations show that qualitatively and quantitatively very similar results are to be expected for the ICE 2 and Shinkansen 300 geometries of Diedrichs *et al.* (2008). We therefore agree with Diedrichs *et al.* (2008) that the difference in the wake flow between the ICE 2 and the Shinkansen 300 is probably the sole reason for the strong lateral vibrations of the Shinkansen 300, without any enhancement by acoustic resonances.

4. Cavity in a cylindrical pipe

In this section we investigate acoustic resonances around a second type of localized feature, namely a cavity in an infinitely long cylindrical pipe of diameter D. Such resonances are usually excited aerodynamically by self-excited shear layers over the mouth of the cavity. Rockwell & Naudascher (1978) classified this as 'fluid – resonant oscillation' which can lead to high-amplitude locked-on states for resonant modes with high quality factor Q, i.e. low radiation loss, possibly causing serious vibration and noise problems (for a recent review of fluid – resonant oscillations see Rockwell *et al.* 2003).

4.1. *Axisymmetric cavity*

In the electromagnetic context axisymmetric cavities are of great importance for example in the design of superconducting linear accelerators where resonances above the first cutoff frequency of the beam tubes having a high quality factor Q may cause beam instabilities, see Schuhmann & Weiland (2000). In the acoustical context of this paper we compute acoustic resonances for the simpler geometry of an axisymmetric cylindrical cavity of length l and depth h in a pipe as sketched in figure 17. Essentially this is a three-dimensional extension of the two-dimensional geometry investigated recently by Duan *et al.* (2007). Such axisymmetric cylindrical cavities can produce high-amplitude narrow-band noise in steam pipe lines caused for example by vortex shedding in open gate valves, see Smith & Luloff (2000) or Lafon *et al.* (2003).

For this axisymmetric problem we again classify resonant modes via the three modal numbers (m, n, ρ). First we fix the cavity height $h/D = 1$ and vary the cavity

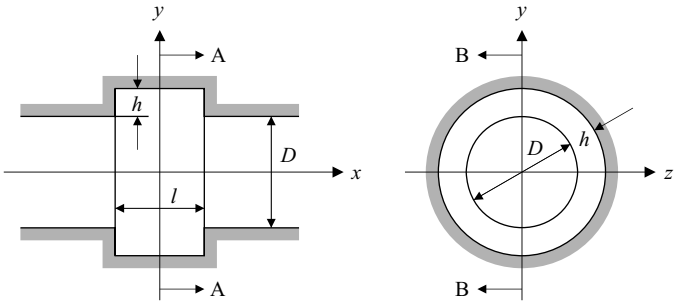

FIGURE 17. Axisymmetric cavity in a circular pipe.

length l/D. In a pipe without a cavity the cutoff frequencies for the (m, ρ) modes in the pipe with diameter D provide an upper limit for trapped modes, whereas the cutoff frequencies for the (m, ρ) modes in the pipe with $D + 2h$, formed by the cavity, give a lower limit. For the $(1, 0)$ duct mode these cutoff limits are marked in figure 18(a) by the dotted and dash-dotted line respectively. The domain of the $(1, n, 0)$ trapped modes lies between these two limits in the shaded area. This can be seen clearly in figure 18(b) where all $(1, n, 0)$ modes have zero damping as long as they are in the shaded domain but become damped once they are above the dotted line for the $(1, 0)$ cutoff frequency in the pipe. However, we notice that at particular values of l/D (and particular frequencies) the resonances also approach zero damping above the first cutoff frequency, strongly indicating the existence of embedded trapped modes. The general appearance is very similar to that of the two-dimensional problem treated by Duan *et al.* (2007) where truly embedded trapped modes were computed semi-analytically via mode matching (probably the same method could be used to compute truly embedded trapped modes in our axisymmetric case). The resonance frequency curves for the $(m, 0, 1)$ modes look similar to the ones for the $(m, 0, 0)$ modes in figure 18(a) but lie at higher $\mathrm{Re}(K/2\pi)$ values. Figure 19 shows sample eigenfunctions for $l/D = 2$ and $h/D = 1$, including the radial eigenfunction $(1, 0, 1)$ at $\mathrm{Re}(K/2\pi) = 0.5695$ which is either a truly trapped mode or a nearly trapped mode with very small imaginary part.

Figure 20 shows the resonant frequencies for a few $(m, n, 0)$ modes with constant cavity length $l/D = 1$ but variable cavity depth h/D. The trapped mode domain of the $(1, n, 0)$ modes between the cutoff frequency $(1, 0)_D$ in the pipe and the cutoff frequency $(1, 0)_{D+2h}$ in the cavity is marked by the shaded area.

4.2. *Side branch cavity*

Next we study acoustic resonances in closed cylindrical side branches of equal diameter d crossing the circular main pipe of diameter D at a right angle as depicted in figure 21. Side branches of equal length $l = l_1 = l_2$ on opposite sides of the main pipe with $l_3 = 0$ are called coaxial side branches or a cross junction, see Ziada & Bühlmann (1992) or Kriesels *et al.* (1995). A single side branch, i.e. $l_2 = l_3 = 0$, is termed a T-junction, see Jungowski, Botros & Studzinski (1989), and tandem side branches are two side branches of length l_1 and l_3 on the same side of the main pipe but a distance s apart with $l_2 = 0$, see Ziada & Bühlmann (1992), Ziada & Shine (1999), Dequand *et al.* (2003).

A related electromagnetic problem of coupled circular waveguides has been investigated recently by Annino *et al.* (2006). They used a finite-element method with

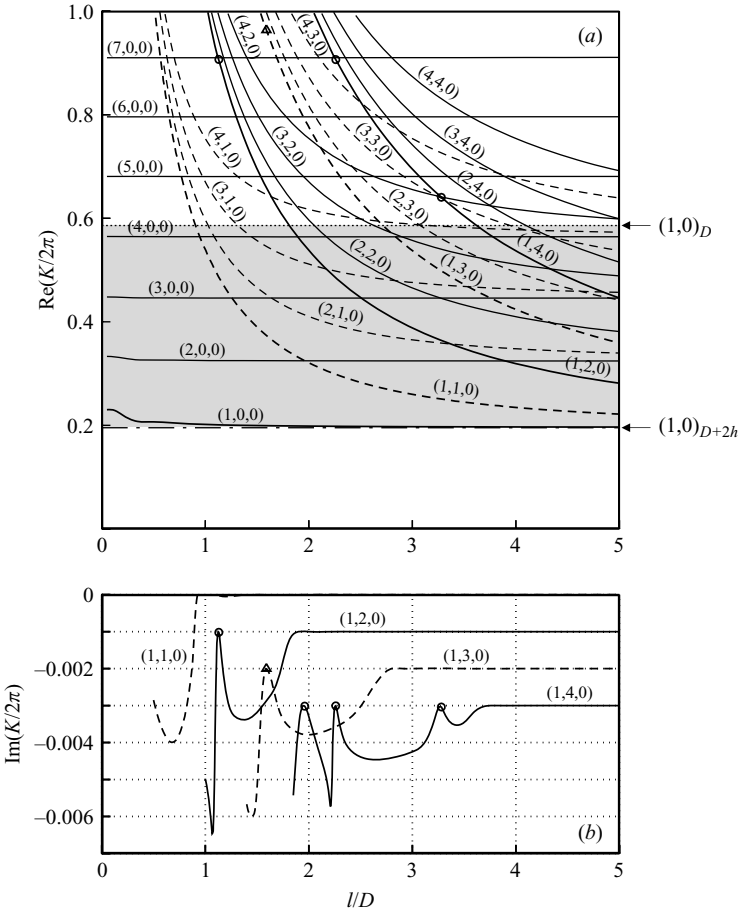

FIGURE 18. Axisymmetric cavity with $h/D = 1$: (*a*) resonant frequencies of the first few $(m, n, 0)$ modes as a function of cavity length l/D. The shaded area marks the domain of the $(1, n, 0)$ trapped modes. Solid lines denote x-symmetric modes, dashed lines x-antisymmetric modes. (*b*) Damping of $(1, n, 0)$ modes with $n = 0, \ldots, 4$. (To distinguish the individual curves the origin of each curve is shifted by -0.001). The symbols mark possible embedded trapped modes above the first cutoff frequency. $p = 2$, $d_{PML} = 4$, $\sigma_0 = 1$.

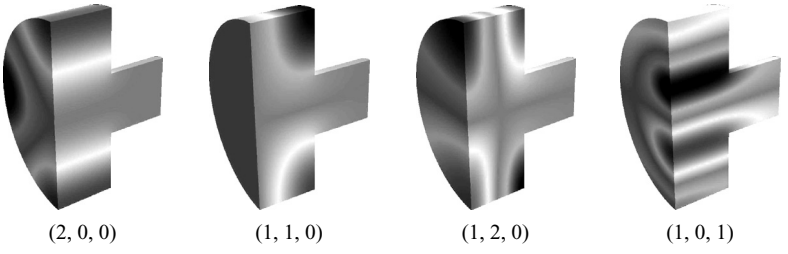

FIGURE 19. Axisymmetric cavity with $h/D = 1$ and $l/D = 2$: sample eigenfunctions of x-symmetric and x-antisymmetric resonances (m, n, ρ). Depicted are the eigenfunctions $\mathrm{Re}(\phi)$ on the surface of the quarter-problem $x \geqslant 0$, $z \leqslant 0$ up to $x_{PML} = 2$.

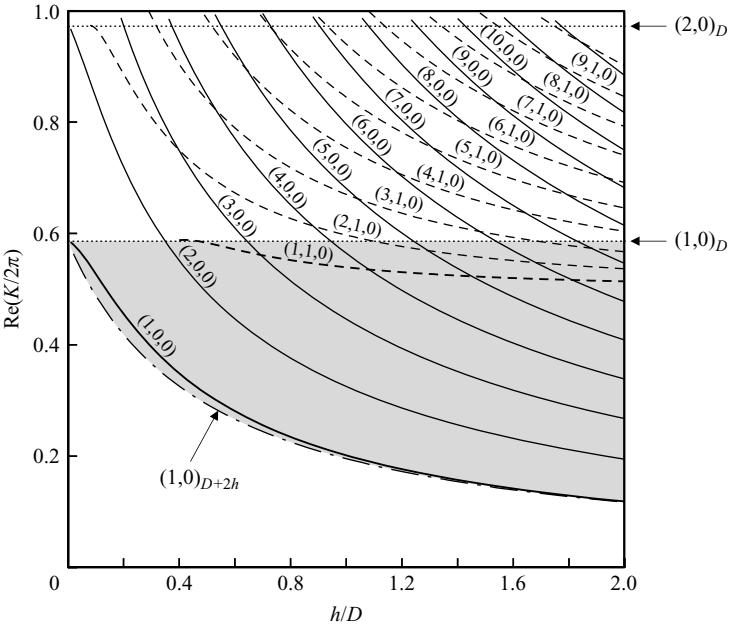

FIGURE 20. Axisymmetric cavity with $l/D = 1$: resonant frequencies of the first few $(m, n, 0)$ modes as a function of cavity depth h/D. The shaded area marks the domain of the $(1, n, 0)$ trapped modes. Solid lines denote x-symmetric modes, dashed lines x-antisymmetric modes. $p = 2$, $d_{PML} = 4$, $\sigma_0 = 1$.

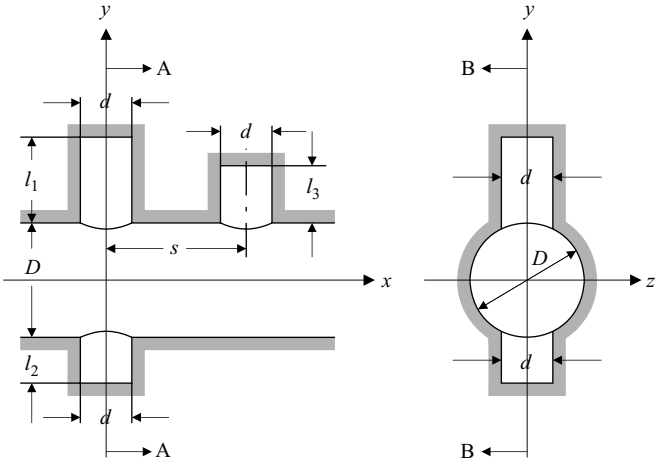

FIGURE 21. Side branch cavities in a circular pipe.

PMLs similar to ours and corroborated their theoretical results experimentally. Such waveguide crossings are of particular importance for so-called quantum wires, see the literature cited in Annino *et al.* (2006). In quantum wires, with Dirichlet boundary conditions instead of the Neumann boundary conditions of acoustics, trapped modes are termed *bound states* and can be sustained at the intersection of two waveguides below the cutoff frequency of either waveguide. Unlike this, in our acoustical problem trapped modes are formed by cavity resonances in the closed side branches of the

main pipe. Below the cutoff frequency of the main pipe such trapped modes are usually excited aerodynamically by self-excited shear layers at the opening of the side branches and can lead to severe vibration and noise problems in gas and steam pipe lines, see for example Jungowski *et al.* (1989), Ziada & Bühlmann (1992), Kriesels *et al.* (1995), Ziada & Shine (1999) and references cited therein. Above the first cutoff frequency of the main pipe embedded trapped modes are possible only if the cavity modes do not couple with the cuton modes of the main pipe. Necessarily, this can occur only under very special conditions and for very particular frequencies, see the remark in Duan *et al.* (2007) for two-dimensional wave guides. Up to now we have found no conclusive evidence of embedded trapped modes for side branches above the cutoff frequency of the main pipe. However, nearly trapped mode resonances with very low damping may also be of importance in engineering applications.

4.2.1. *Symmetric cross junction*

First we investigate resonances in a so-called symmetric cross junction with side branches of equal length $l = l_1 = l_2$ on opposite sides of the main pipe, as examined experimentally by Ziada & Bühlmann (1992) and Kriesels *et al.* (1995). We arbitrarily fix $d/D = 0.5$ and vary the side branch length l/D. According to Ziada & Shine (1999) coaxial side branches of equal length produce the strongest resonance and have the lowest radiation loss. Due to symmetries about the three axes we can confine our computation to the octant $x \geqslant 0$, $y \geqslant 0$, $z \geqslant 0$ by applying appropriate symmetry conditions at $x = 0$, $y = 0$ and $z = 0$. As for the closed ball-type valve of § 3.2 we denote a mode by SAS if it is symmetric in x, antisymmetric in y and symmetric in z, and so on. Figure 22 shows the lowest SAS resonances as a function of side branch length l/D. Essentially these are the acoustic modes with an odd number of quarter-wavelengths in one side branch

$$L^* f^*/c_0^* = (1/4 + n/2), \qquad n = 0, 1, 2, \ldots, \tag{4.1}$$

as defined by Jungowski *et al.* (1989), Ziada & Bühlmann (1992) and Kriesels *et al.* (1995).

The open question remains of what to take as L^*. Kriesels *et al.* (1995) define L^* as the distance from the axis of the main pipe to the end of the side branch. The corresponding odd number $\lambda/4$ resonances are shown by the dotted curves in figure 22(*a*). The odd number $\lambda/4$ resonances with L^* equalling the side branch length l^*, as defined by Ziada & Bühlmann (1992), are depicted by the dashed curves. We see that up to the first cutoff frequency $(1, 0)_D$ in the main pipe the actual resonances, depicted by the solid curves, are between these two approximations. This is in accordance with the findings of Kriesels *et al.* (1995), who mention that $\lambda/4 > l$. Below the first cutoff frequency $(1, 0)_D$ the imaginary parts of the $\lambda/4$ resonances are less than 10^{-9} almost uniformly throughout the shaded domain in figure 22(*a*). Although this is no proof, it is a strong indication that these $\lambda/4$ resonances are truly trapped modes, which agrees with the statement of Ziada & Shine (1999) that coaxial branches of equal length have negligible radiation loss into the main pipe. Near the first cutoff frequency $(1, 0)_D$ the efficiency and hence the accuracy of our PML deteriorates as can be seen from the slight oscillations in figure 22(*b*) near the cutoff frequency. Above the first cutoff frequency $(1, 0)_D$ the $\lambda/4$ resonances are strongly damped due to radiation losses as can be seen clearly in figure 22(*b*). The y-symmetric modes SSS are always damped because they can radiate through the main pipe via the fundamental pipe mode (0, 0) (see the solid symbols at $l_2/l_1 = 1$ in figure 23(*b*)).

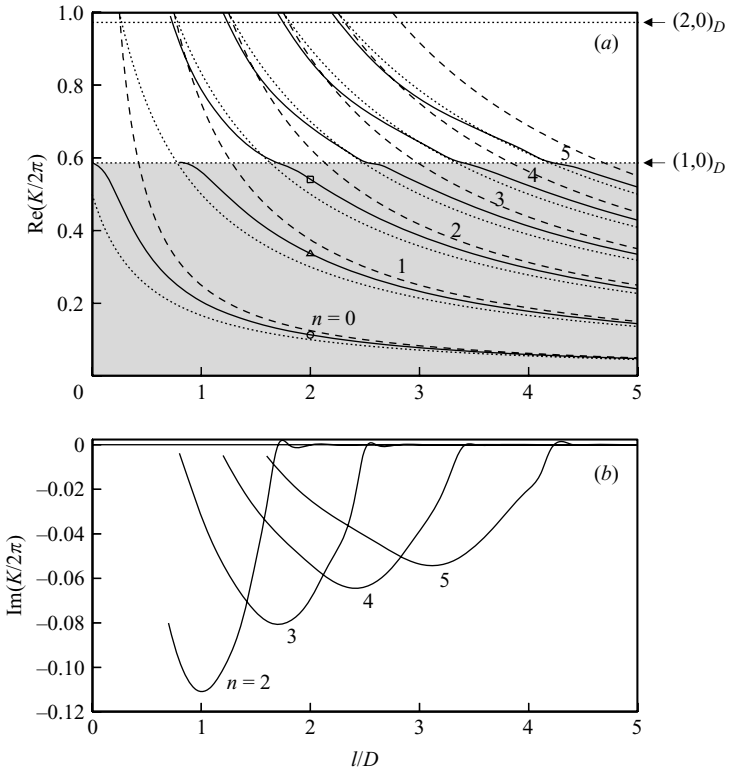

FIGURE 22. Symmetric cross junction with $d/D = 0.5$. (a) Resonant SAS frequencies of first six $(2n+1)\lambda/4$ modes as a function of side branch length l/D. The shaded area marks the domain of possibly trapped modes. Dotted curves denote approximation of resonant frequencies with $(2n+1)\lambda/4 = l + 1/2$, dashed curves denote approximation of resonant frequencies with $(2n+1)\lambda/4 = l$, $n = 0, 1, \ldots$. (b) Radiation damping of $(2n+1)\lambda/4$ modes with $n = 2$ up to $n = 5$ computed with $p = 2$, $x_{PML} = 1.2$, $d_{PML} = 4$, $\sigma_0 = 1$.

As pointed out by a referee experimental results of Kriesels *et al.* (1995) demonstrate that the higher harmonics of the resonance are associated with significant radiation losses. Figure 22 shows that above the cutoff frequency $(1, 0)_D$ considerable damping occurs which agrees with these experimental observations.

4.2.2. *Asymmetric cross junction*

Next we fix $d/D = 0.5$ and the length $l_1/D = 2$ of the first side branch and vary the length l_2/D of the second side branch. Now the problem is no longer symmetric or antisymmetric about $y = 0$ and we limit our computation to the quarter-problem $x \geqslant 0, z \geqslant 0$ by applying symmetry conditions at $x = 0$ and $z = 0$. The x-symmetric, z-symmetric (SS) results are shown in figure 23. Starting with $l_2/l_1 = 1$, i.e. the symbols in figure 22(a), we see that all three (possibly trapped) SAS modes below the cutoff frequency $(1, 0)_D$ become damped when $l_2/l_1 \neq 1$. On the other hand the SSS modes of the symmetric cross junction below the cutoff frequency $(1, 0)_D$, depicted by the filled symbols at $l_2/l_1 = 1$, are already damped as mentioned above. On moving away from $l_2/l_1 = 1$ one resonance frequency remains more or less constant whereas the other varies until it almost coincides with one of the neighbouring constant frequencies. At these special points, marked by the cross symbols in figure 23, isolated trapped modes seem to exist. They correspond roughly to the condition where there

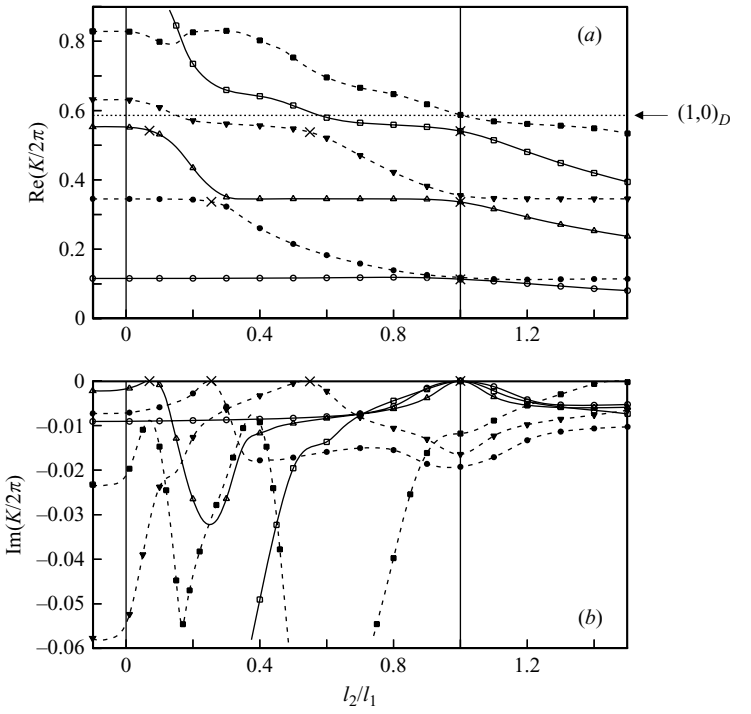

FIGURE 23. Asymmetric cross junction with $d/D = 0.5$ and $l_1/D = 2$: (*a*) resonant frequencies and (*b*) radiation damping of the first few x-symmetric, z-symmetric modes as a function of l_2/l_1. The solid curves with the open symbols start at the SAS modes of figure 22(*a*) at $l/D = 2$, the curves with the filled symbols correspond to the SSS modes. All are computed with $p = 2$, $x_{PML} = 1.2$, $d_{PML} = 4$, $\sigma_0 = 1$.

are $(2n + 1)\lambda/4$ wavelengths in side branch 1 and $(2\nu + 1)\lambda/4$ wavelengths in side branch 2, $n, \nu = 0, 1, 2, \ldots$.

From this one concludes that asymmetry of the cross junction side branches damps oscillations, but only away from the trapped mode points mentioned above. It is also interesting to note that the mode above the cutoff frequency $(1, 0)_D$ in figure 23, i.e. the curve with the filled squares for $l_2/l_1 < 1$, has two damping minima which are clearly below zero, contrary to the isolated trapped mode values of the modes whose frequency is below the cutoff frequency $(1, 0)_D$.

4.2.3. *Tandem side branches*

The second example where Ziada & Bühlmann (1992) observed large-amplitude oscillations in their experiments were tandem side branches with $l = l_1 = l_3$ and $l_2 = 0$. Therefore, we compute the resonances in such equal-length tandem side branches in this section. We fix $l/D = 2, d/D = 0.5$ and vary the distance s/D between the two side branches, see figure 21. By applying symmetry conditions at $x = 0$, which for the case of equal-length side branches is chosen halfway between the two side branches, and $z = 0$ we can limit our computations to the quarter-problem $x \geqslant 0, z \geqslant 0$.

The first five x-symmetric, z-symmetric resonances SS are depicted in figure 24 for $0 \leqslant s/D \leqslant 5$. At $s/D = 0.5$ the two side branches touch each other forming a single side branch with non-circular cross-section. Between $s/D = 0$ and $s/D = 0.5$, marked by the shaded area in figure 24, the two side branches are no longer separated

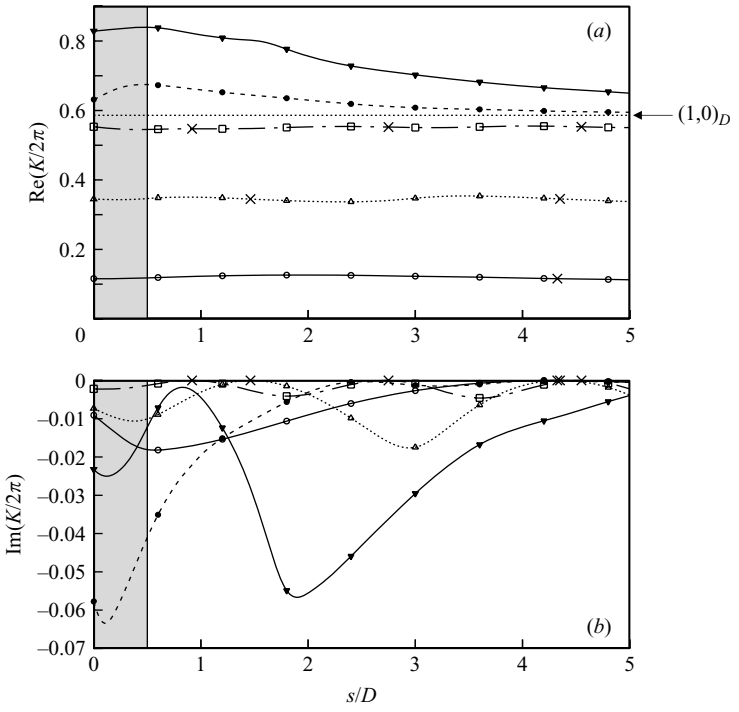

FIGURE 24. x-symmetric, z-symmetric tandem side branches of equal length $l/D = 2$ with $d/D = 0.5$: (a) resonant frequencies and (b) radiation damping of the first five SS modes as a function of distance s/D between the two branches computed with $p = 2$, $d_{PML} = 4$, $\sigma_0 = 1$.

by the main pipe in the x-direction. However, as can be seen, the x-symmetric resonances of the single side branch with non-circular cross-section constitute the natural continuation of the tandem mode resonances. At $s/D = 0$ the side branch reduces to a single side branch with circular cross-section (T-junction). Note that all T-junction modes are damped. The resonant frequencies $\mathrm{Re}(K/2\pi)$ are determined by the length of the side branches and therefore remain almost constant (at least below the first cutoff frequency $(1,0)_D$ of the main pipe). On the other side, the damping $\mathrm{Im}(K/2\pi)$ varies considerably depending on the distance s between the tandem branches. The damping reaches vanishingly small values at the few tuned values marked by the cross symbols in figure 24. By refining s/D iteratively near these tuned values the damping of the resonances below $(1,0)_D$ can be reduced to very small values, indicating that probably the corresponding modes are truly trapped. For the x-symmetric modes of figure 24 these tuned values occur at approximately $s/D = (2n-1)\lambda/2$, $n = 1, 2, \ldots$, as suggested by Ziada & Bühlmann (1992). At these tuned frequencies the eigenfunction amplitude has a maximum at $x = 0$.

Figure 25 depicts the first five x-antisymmetric, z-symmetric resonances AS. Unlike the x-symmetric modes of figure 24 the curves are discontinued at $s/D = 0.5$ because for $s/D < 0.5$ the solution is antisymmetric in the side branch with non-circular cross-section and not in the main pipe. Therefore, this is a completely different solution. For $s/D \geqslant 0.5$ the resonant frequencies $\mathrm{Re}(K/2\pi)$ are again determined by the length of the side branches. The tuned values, marked by the cross symbols in figure 25, are now approximately at $s/D = n\lambda$, $n = 1, 2, \ldots$. The damping $\mathrm{Im}(K/2\pi)$ at these tuned frequencies is again vanishingly small, suggesting that the modes at these tuned

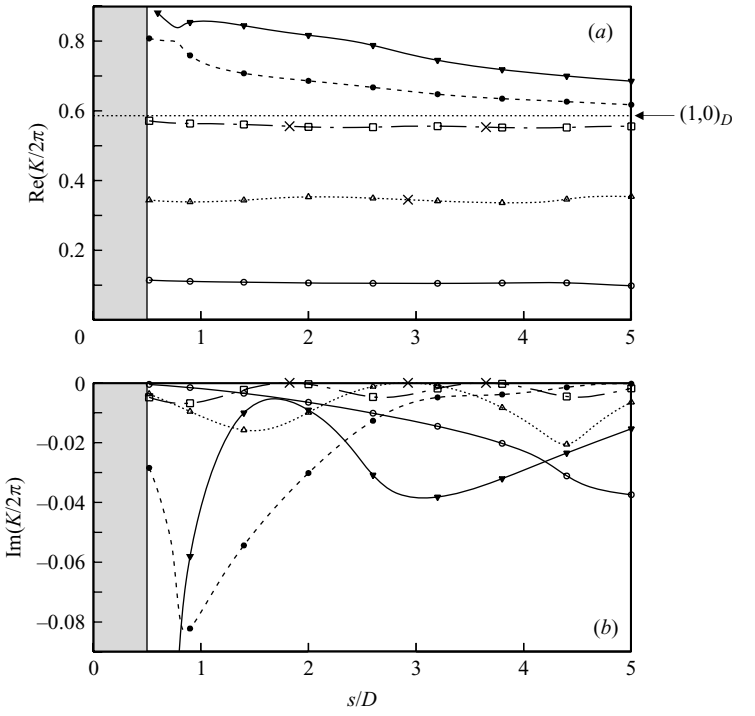

FIGURE 25. x-antisymmetric, z-symmetric tandem side branches of equal length $l/D = 2$ with $d/D = 0.5$: (a) resonant frequencies and (b) radiation damping of the first five AS modes as a function of distance s/D between the two branches computed with $p = 2$, $d_{PML} = 4$, $\sigma_0 = 1$.

frequencies below the first cutoff frequency $(1, 0)_D$ of the main pipe are truly trapped with a node at $x = 0$. The modes above the cutoff frequency $(1, 0)_D$ have distinct minima in $\mathrm{Im}(K/2\pi)$ which are not vanishingly small and therefore these modes are only nearly trapped.

The experiments of Jungowski *et al.* (1989) have shown that increasing the diameter d of a T-junction side branch, keeping the diameter D of the main pipe fixed, leads to a rapid reduction in the pulsation amplitude at resonance due to increased radiation losses into the main pipe. In the following we vary d/D for a single side branch to see whether this is corroborated by our resonance computation. The results for the first five x-symmetric, z-symmetric SS modes are shown in figure 26. The damping does indeed increase as d/D increases, whereas the resonant frequencies remain fairly constant. This is true at least for the modes below the first cutoff frequency $(1, 0)_D$ of the main pipe. For the modes above $(1, 0)_D$ the damping first increases with increasing d/D, reaches a maximum and then decreases again.

Summarizing, we can state that the trends experimentally found by Ziada & Bühlmann (1992), Ziada & Shine (1999) and Jungowski *et al.* (1989), namely that the radiation losses are lowest for a symmetric cross junction, and that the radiation losses of a T-junction increase with increasing d/D, are reproduced by our resonance computations as long as one considers the resonances whose frequencies are below the first cutoff frequency of the main pipe. Some of the resonances appear to have zero radiation losses, i.e. might be truly trapped, and the experimental results seem to indicate that these resonances indeed control the shear-layer sound source by lock-on.

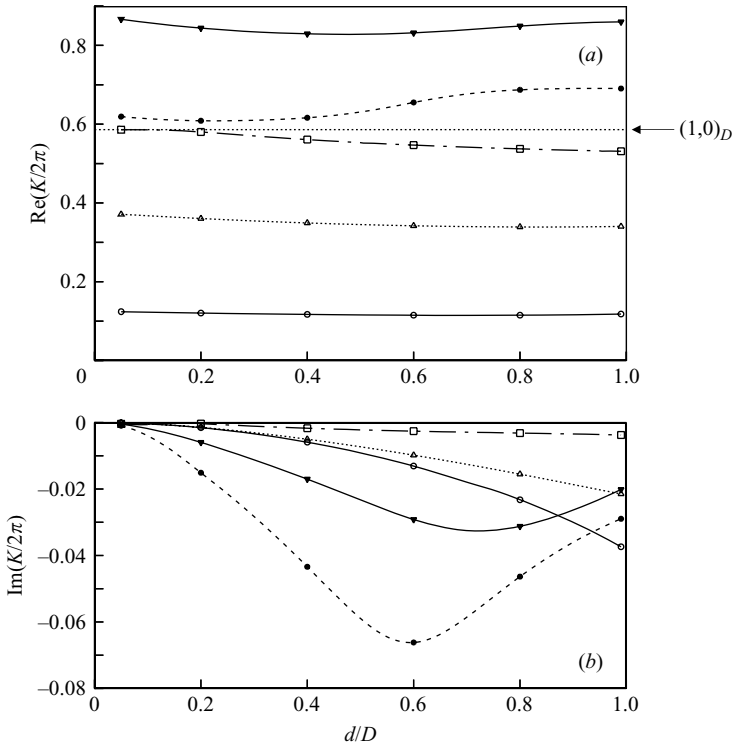

FIGURE 26. Variation of d/D for a single side branch with $l/D = 2$: (a) resonant frequencies and (b) radiation damping of the first five SS modes with $p = 2$, $d_{PML} = 4$, $\sigma_0 = 1(2)$.

5. Conclusion

Using perfectly matched layer absorbing boundary conditions in the form of the complex scaling method, acoustic resonances were computed numerically for various three-dimensional sound-hard structures of finite length in an infinitely long pipe. Such resonances can be excited by self-sustaining shear-layer oscillations. In particular, spheres, cylinders, cavities and closed side branches, located on the pipe centreline or off-centre, were studied. Several resonances with vanishingly small damping could be identified as truly trapped modes with zero radiation loss. We cannot prove the existence of a truly trapped mode with our numerical method, but in practice it makes no difference whether the resonance has exactly zero radiation loss (trapped mode) or merely very small damping (nearly trapped mode). In this context it is of interest to note that if a symmetric three-dimensional object moves off the centreline of the pipe one mode becomes a damped resonance as in two dimensions whereas the other mode remains nearly trapped or perhaps truly trapped.

Usually trapped modes have a frequency below the first cutoff frequency of the pipe, but for very special geometries of axisymmetric cavities we also found strong evidence for the existence of isolated embedded trapped modes above the first cutoff frequency. Furthermore, our results for closed side branches indicate that the resonant modes of side branch configurations for which negligible radiation losses were observed in experiments are in fact truly trapped modes. In applying our method to the computation of acoustic resonances around a model high-speed train in an infinitely long double-track tunnel we showed the existence of nearly trapped modes. However,

their resonant frequency is one order of magnitude too high to enhance the lateral vibrations of the tail vehicle which have been observed with the Japanese Shinkansen 300 high-speed train.

We are grateful to Joachim Schöberl for making available to us his finite-element code NGSolve. Furthermore, we appreciated the helpful comments and suggestions of the three referees.

REFERENCES

Aguilar, J. & Combes, J. M. 1971 A class of analytic perturbations for one-body Schrödinger Hamiltonians. *Commun. Math. Phys.* **22**, 269–279.

Annino, G., Yashiro, H., Cassettari, M. & Martinelli, M. 2006 Properties of trapped electromagnetic modes in coupled waveguides. *Phys. Rev.* B **73**, 125308-1–125308-8.

Aslanyan, A., Parnovski, L. & Vassiliev, D. 2000 Complex resonances in acoustic waveguides. *Q. J. Mech. Appl. Maths* **53**, 429–447.

Baslev, E. & Combes, J. M. 1971 Spectral properties of many body Schrödinger operators with dilation analytic interactions. *Commun. Math. Phys.* **22**, 280–294.

Bearman, P. W. 1984 Vortex shedding from oscillating bluff bodies. *Annu. Rev. Fluid Mech.* **16**, 195–222.

Bérenger, J. P. 1994 A perfectly matched layer for the absorption of electromagnetic waves. *J. Comput. Phys.* **114**, 185–200.

Callan, M., Linton, C. M. & Evans, D. V. 1991 Trapped modes in two-dimensional waveguides. *J. Fluid Mech.* **229**, 51–64.

Camp, T. R. 1999 A study of acoustic resonance in a low-speed multistage compressor. *Trans. ASME: J. Turbomachinery* **121**, 36–43.

Chew, W. C. & Weedon, W. H. 1994 A 3-D perfectly matched medium from modified Maxwell's equation with stretched coordinates. *Microwave Optical Technol. Lett.* **7**(13), 599–604.

Collino, F. & Monk, P. 1998 The perfectly matched layer in curvilinear coordinates. *SIAM J. Sci. Comput.* **19**, 2061–2090.

Dequand, S., Hulshoff, S. J. & Hirschberg, A. 2003 Self-sustained oscillations in a closed side branch system. *J. Sound Vib.* **265**, 359–386.

Diedrichs, B., Krajnović, S. & Berg, M. 2008 On the aerodynamics of car body vibrations of high-speed trains cruising inside tunnels. *Engng. Appl. Comput. Fluid Mech.* **2**, 51–75.

Duan, Y., Koch, W., Linton, C. M. & McIver, M. 2007 Complex resonances and trapped modes in ducted domains. *J. Fluid Mech.* **571**, 119–147.

Duan, Y. & McIver, M. 2004 Rotational acoustic resonances in cylindrical waveguides. *Wave Motion* **39**, 261–274.

Duclos, P., Exner, P. & Šťovíček, P. 1995 Curvature-induced resonances in a two-dimensional Dirichlet tube. *Ann. Inst. Henri Poincaré* **A62**, 81–101.

Evans, D. V. & Linton, C. M. 1991 Trapped modes in open channels. *J. Fluid Mech.* **225**, 153–175.

Evans, D. V. & Porter, R. 1998 Trapped modes embedded in the continuous spectrum. *Q. J. Mech. Appl. Maths* **52**, 263–274.

Harari, I., Patlashenko, I. & Givoli, D. 1998 Dirichlet-to-Neumann maps for unbounded wave guides. *J. Comput. Phys.* **143**, 200–223.

Hein, S., Hohage, T. & Koch, W. 2004 On resonances in open systems. *J. Fluid Mech.* **506**, 255–284.

Hein, S., Hohage, T., Koch, W. & Schöberl, J. 2007 Acoustic resonances in a high lift configuration. *J. Fluid Mech.* **582**, 179–202.

Hislop, P. D. & Sigal, I. M. 1996 *Introduction to Spectral Theory*. Springer.

Hu, F. Q. 2004 Absorbing boundary conditions. *Intl. J. Comput. Fluid Dyn.* **18**, 513–522.

Jungowski, W. M., Botros, K. K. & Studzinski, W. 1989 Cylindrical side-branch as tone generator. *J. Sound Vib.* **131**, 265–285.

Koch, W. 1983 Resonant acoustic frequencies of flat plate cascades. *J. Sound Vib.* **88**, 233–242.

Kriesels, P. C., Peters, M. C. A. M., Hirschberg, A., Wijnands, A. P. J., Iafrati, A., Riccardi, G., Piva, R. & Bruggeman, J. C. 1995 High amplitude vortex-induced pulsations in a gas transport system. *J. Sound Vib.* **184**, 343–368.

Lafon, P., Caillaud, S., Devos, J. P. & Lambert, C. 2003 Aeroacoustical coupling in a ducted shallow cavity and fluid/structure effects on a steam line. *J. Fluids Struct.* **18**, 695–713.

Levitin, M. & Marletta, M. 2006 A simple method of calculating eigenvalues and resonances in domains with regular ends. ArXiv preprint math.SP/0611237.

Li, Y. & Mei, C. C. 2006 Subharmonic resonance of a trapped wave near a vertical cylinder in a channel. *J. Fluid Mech.* **561**, 391–416.

Linton, C. M. & McIver, M. 1998 Trapped modes in cylindrical waveguides. *Q. J. Mech. Appl. Maths* **51**, 389–412.

Linton, C. M. & McIver, P. 2007 Embedded trapped modes in water waves and acoustics. *Wave Motion* **45**, 16–29.

Mittra, R. & Lee, S. W. 1971 *Analytical Techniques in the Theory of Guided Waves*. Macmillan.

Moiseyev, N. 1998 Quantum theory of resonances: calculating energies, widths and cross-sections by complex scaling. *Phys. Rep.* **302**, 211–293.

Nayfeh, A. H. & Huddleston, D. H. 1979 Resonant acoustic frequencies of parallel plates. *AIAA Paper* 79-1522.

Parker, R. 1966 Resonance effects in wake shedding from parallel plates: Some experimental observations. *J. Sound Vib.* **4**, 62–72.

Parker, R. 1967*a* Resonance effects in wake shedding from compressor blading. *J. Sound Vib.* **6**, 302–309.

Parker, R. 1967*b* Resonance effects in wake shedding from parallel plates: Calculation of resonant frequencies. *J. Sound Vib.* **5**, 330–343.

Parker, R. 1984 Acoustic resonances and blade vibration in axial flow compressors. *J. Sound Vib.* **92**, 529–539.

Parker, R. & Stoneman, S. A. T. 1989 The excitation and consequences of acoustic resonances in enclosed fluid flow around solid bodies. *Proc. Inst. Mech. Engrs.* **203**, 9–19.

Rockwell, D., Lin, J.-C., Oshkai, P., Reiss, M. & Pollack, M. 2003 Shallow cavity flow tone experiments: onset of locked-on states. *J. Fluids Struct.* **17**, 381–414.

Rockwell, D. & Naudascher, E. 1978 Review – Self-sustaining oscillations of flow past cavities. *Trans. ASME: J. Fluids Engng.* **100**, 152–165.

Rockwell, D. & Naudascher, E. 1979 Self-sustained oscillations of impinging free shear layers. *Annu. Rev. Fluid Mech.* **11**, 67–94.

Schöberl, J. 1997 NETGEN An advancing front 2D/3D-mesh generator based on abstract rules. *Computing and Visualization in Science* **1**, 41–52.

Schuhmann, R. & Weiland, T. 2000 Rigorous analysis of trapped modes in accelerating cavities. *Phys. Rev. Special Topics—Accelerators and Beams* **3**, 122002.

Simon, B. 1973 The theory of resonances for dilation analytic potentials and the foundations of time dependent perturbation theory. *Ann. Maths* **97**, 247–274.

Smith, B. A. W. & Luloff, B. V. 2000 The effect of seat geometry on gate valve noise. *Trans. ASME: J. Pressure Vessel Technol.* **122**, 401–407.

Suzuki, M. 2004 An aerodynamic design of high-speed train for reducing flow-induced vibration in tunnel. In *Proc. ECCOMAS 2004, Jyväskylä, Finland, July 24–28* (ed. P. Neittaanmäki, T. Rossi, S. Korotov, E. Oñate, J. Périaux & D. Knörzer).

Taylor, M. 1996 *Partial Differential Equations II*. Springer.

Ursell, F. 1991 Trapped modes in a circular cylindrical acoustic waveguide. *Proc. R. Soc. Lond.* A **435**, 575–589.

Ziada, S. & Bühlmann, E. T. 1992 Self-excited resonances of two side-branches in close proximity. *J. Fluids Struct.* **6**, 583–601.

Ziada, S. & Shine, S. 1999 Strouhal numbers of flow-excited acoustic resonance of closed side branches. *J. Fluids Struct.* **13**, 127–142.